Transition-Metal Borides with the Ta_3B_4 Crystal Structure: Their Electronic and Bonding Properties

Ruslan M. Minyaev and Roald Hoffmann*

Department of Chemistry and Materials Science Center, Cornell University, Baker Laboratory, Ithaca, New York 14853-1301, and the Institute of Physical and Organic Chemistry, Rostov University, Rostov-on-Don 344711, USSR

Received July 19, 1990. Revised Manuscript Received January 18, 1991

The electronic structure of transition-metal borides M_3B_4 with the Ta_3B_4 crystal structure has been examined. These materials contain one-dimensional polyacene-type boron chains embedded in a three-dimensional tantalum lattice. The origin of the different bond lengths in the boron double chain is traced. It depends on the electron count in the systems: for the d^3–d^5 metals the shortest B–B length is the interchain bond, and for the late d^6–d^7 transition metals the situation is reversed. The metal–metal and metal–boron interaction for d^6–d^{10} transition metals is strongly antibonding, which leads to their instability.

The borides of the transition metals attract our attention by their special properties, which distinguish them from other borides. The TMB (transition-metal borides) have high melting points, are very hard, and possess high thermal electric conductivity. Some of them become superconducting at low temperatures. The TMB exhibit great thermal stability, and they are not attacked by dilute acids and bases or by concentrated mineral acids. They display considerable resistance to oxidation in air. These properties make the TMB most useful in modern technology. There are several comprehensive books on the chemical and physical properties of the borides,[1-13] where the extensive literature is presented.

At present, the binary, ternary, and other TMB of almost all early and late transition metals are available. But there are also exceptions. The borides of the group IB and IIB transition-metal element subgroups are practically unknown. In Table I we list the currently known well-characterized binary TMB.[1-13] There is a variety of structures in these, boron atoms forming chains, layers, or three-dimensional networks extending throughout the whole crystal. It is this structural richness, achieved by boron–boron bonding, that made us undertake a study of their electronic structure.

In spite of the aforementioned extensive experimental attention devoted to the borides, there are comparatively few theoretical investigations of the electronic structure of the TMB.[14-25] The structural stability of the borides with AlB_2 and related structures is treated incisively in the literature.[14-17] The electronic and structural properties of the TMB (M = Sc–Cu) with the crystal structures of FeB, CrB, NaCl, CsCl, and CuAu, with a zigzag boron chain extending through the crystal, have been studied;[18,19,22,23] monoborides OsB and InB with the WC structure have been investigated by the X_α method in cluster models.[21] The borides CrB_4 and MnB_4, containing tetrahedral carbon nets formed by boron atoms, have been recently studied by Burdett and Canadell.[24] The electronic structure of the boron Kagomé net, a two-dimensional planar geometry characteristic of a number of intermetallic compounds, has been determined and compared with topologically related graphite and close-packed nets by our group.[25]

The subject of this paper is the remarkable Ta_3B_4 structure and its stability and bonding. In this TMB the boron atoms form a sublattice totally unlike that of elemental boron, for Ta_3B_4 has B–B bonded double chains resembling polyacene. We will endeavor to answer the following questions: What is the nature of B–B bonding, and why are there great differences in that bonding depending on metal? Are these really three-dimensional materials? Is there a reason why the late transition metal (such as Cu, Zn) M_3B_4 stoichiometries are unknown?

We will proceed in four steps. First we will consider the Ta_3B_4 structure. In the second and third steps we will consider the electronic properties and relative stability of the boron and tantalum substructures separately. Finally the effects of the interaction of the boron and tantalum

* To whom correspondence should be addressed.

(1) Schwarzkopf, P.; Kieffer, R.; Leszynski, W.; Benesovsky, K. *Refractory Hard Metals, Borides, Carbides, Nitrides, and Silicides*; MacMillan Company: New York, 1953.
(2) Samsonov, G. V.; Markovskii, L. Ya.; Zhigach, A. F.; Valyashko, M. B. *Boron, its Compounds and Alloys*; AN Ukr SSR Publishers: Kiev, 1960.
(3) Aronsson, B.; Lundström, T.; Rundqvist, S. *Borides, Silicides and Phosphides*; Wiley: New York, 1965.
(4) *Boron, Metallo-Boron Compounds and Boranes*; Adams, R. M., Ed.; Interscience: New York, 1964.
(5) Pearson, W. B. *Crystal Chemistry and Physics of Metals and Alloys*; Wiley: New York, 1972.
(6) *Boron and Refractory Borides*; Matkovich, V. I., Ed.; Springer-Verlag: New York, 1977.
(7) Wells, A. F. *Structural Inorganic Chemistry*; Clarendon Press: Oxford, 1975.
(8) Samsonov, G. V.; Goryachev, Yu. M.; Kovenskaya, B. A. J. *Less.-Common Met.* **1976**, *47*, 147.
(9) Lipscomb, W. N. *J. Less-Common. Met.* **1981**, *82*, 1.
(10) Kuz'ma, Yu. B. *Crystallochemistry of Borides*; L'vov University Publishers: L'vov, USSR, 1983.
(11) Villars, P.; Carvert, L. D.; *Pearson's Handbook of Crystallographic Data for Intermetallic Phases*; Americal Society for Metals: Metals Park, OH, 1985; Vol 2.
(12) Hyde, B. G.; Andersson, S.; *Inorganic Crystal Structures.*; Wiley: New York, 1989.
(13) Fehlner, T. P. *The Metal Face of Boron*, in press.
(14) Burdett, J. K.; Canadell, E.; Miller, G. J. *J. Am. Chem. Soc.* **1986**, *108*, 6561.
(15) Armstrong, D. R. *Theor. Chim. Acta* **1983**, *64*, 137.
(16) Ihara, H.; Hirabayashi, M.; Nakagawa, H. *Phys. Rev. B: Solid State Phys.* **1977**, *B16*, 726.
(17) Liv, S. H.; Kopp, L.; England, W. B.; Myron, H. W. *Phys. Rev. B: Solid State Phys.* **1975**, *B11*, 3463.
(18) Mohn, P.; Pettifor, D. G. *J. Phys. C: Solid State Phys.* **1988**, *21*, 2829.
(19) Pettifor, D. G.; Podloucky, R. *J. Phys. C: Solid State Phys.* **1986**, *19*, 315.
(20) Mohn, P. *J. Phys. C: Solid State Phys.* **1988**, *21*, 2841.
(21) Novikov, D. L.; Ivanovskii, A. L.; Gubanov, V. A. *Zh. Neorg. Khim.* **1988**, *33*, 2673.
(22) Armstrong, D. R.; Perkins, P. G.; Centina, V. E. *Theor. Chim. Acta* **1983**, *64*, 41.
(23) Perkins, P. G.; Sweeney, A. V. J. *J. Less-Common Met.* **1976**, *47*, 165.
(24) Burdett, J. K.; Canadell, E. *J. Am. Chem. Soc.* **1988**, *27*, 4437.
(25) (a) Wheeler, R. A.; Hoffmann, R., unpublished. (b) Johnston, R. L.; Hoffmann, R., unpublished.

0897-4756/91/2803-0547$02.50/0

Table I. Well-Characterized Binary Transition-Metal Borides

ScB_2	TiB	V_3B_2	Cr_4B	Mn_4B	$Fe_{23}B_6$	Co_3B	Ni_3B	CuB_{23}	Zn
ScB_6	TiB_2	VB	Cr_2B^a	Mn_2B	Fe_3B^a	Co_2B	Ni_7B_3	CuB_{28}	
ScB_{12}	Ti_3B_4	V_5B_6	Cr_5B_3	MnB	Fe_2B	CoB	Ni_2B		
ScB_6	Ti_2B_5	V_3B_4	CrB	Mn_3B_4	FeB	CoB_{20}	$Ni_4B_3^a$		
ScB_{28}	TiB_{20}	V_2B_3	Cr_3B_4	MnB_2	$FeB_{29.5}$		NiB		
	TiB_{25}	VB_2	CrB_2	MnB_4^a	FeB_{49}		NiB_{12}		
			CrB_4	MnB_{23}			NiB_{20}		
			CrB_6						
			CrB_{41}						
YB_2	ZrB	Nb_3B_2	Mo_2B	Tc_3B	Ru_7B_3	Rh_7B_3	$Pd_{16}B_3$	Ag	Cd
YB_3	ZrB_2	NbB	Mo_3B_2	Tc_7B_3	$Ru_{11}B_8$	$RhB_{1.1}$	Pd_3B		
YB_4	ZrB_{12}	Nb_3B_4	MoB^a	TcB_2	RuB^a		Pd_2B		
YB_6	ZrB_{51}	NbB_2	MoB_2		$RuB_{1.1}$				
YB_{12}			Mo_2B_5		Ru_2B_3				
YB_{66}			MoB_4		$RuB_{1.5}$				
					RuB_2				
LaB_4	HfB^a	Ta_2B	W_2B	Re_3B	$OsB_{1.2}$	$IrB_{0.9}$	Pt_4B	Au	Hg
LaB_6	HfB_2	Ta_3B_2	WB^a	Re_7B_3	$OsB_{1.5}$	$IrB_{1.1}$	Pt_3B		
	HfB_{12}	TaB	WB_2	ReB_2	Os_2B_3	$IrB_{1.35}$	Pt_2B		
	HfB_{50}	Ta_3B_4	W_2B_5	Re_2B_5	OsB_2	IrB^a	PtB^a		
		TaB_2	WB_2^a	ReB		Ir_4B_5			
			WB_4	Re_3B_7		Ir_3B_4			
			W_2B_9	ReB_3		IrB_{50}			
			WB_{12}						

[a] There is more than one phase or near this composition.

sublattices will be discussed.

As a computational tool we use extended Hückel tight-binding[26] band calculations, with parameters specified in the Appendix. We are aware of the roughness of this approach and also the limitations of conclusions based on extended Hückel calculations.[26] This approximate molecular orbital (MO) procedure is a one-electron method and consequently does not directly include electron correlation or relativistic effects such as are likely to be important for heavy atoms. The method is also not reliable for optimization of bond lengths in molecules or the solid state. Without rehearsing the limitations of the extended Hückel method, we mention those articles[27] that are useful for an understanding of this methodology and in which there are very helpful critical remarks and precautions concerning the application of semiempirical methods.

The Ta_3B_4 Crystal Structure

The Ta_3B_4 crystal structure[28] belongs to the space groups *Immm* (No. 71).[29,30] It has the structure shown in 1.

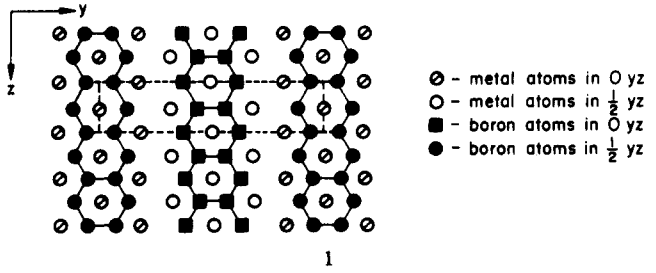

1

Table II. Boron–Boron Distances (angstroms) in Binary Borides with the Ta_3B_4 Crystal Structure

metal	r_B/r_M[a]	$(B-B)_{short}$	$(B-B)_{long}$	ref
Ti	0.59			30
Ta	0.60	1.57	1.85	28a
Nb	0.60	1.58	1.84	28a
V	0.65			29
Cr	0.69	1.69	1.77	28e
Cr	0.69	1.51	1.74	28a
Mn	0.69	1.47	1.75	28a

[a] Ratio of boron to metal covalent radii.

The orthorhombic unit cell of Ta_3B_4 is drawn in 2. Note the two distinct bond distances in the boron chain and four different separations between tantalums. This differentiation is also observed in other M_3B_4 compounds with the Ta_3B_4 structure, which are listed in Table II. The variation of B–B distances in this compounds will be one focus of our study. We note for calibration that a B–B single bond distance is around 1.70–1.74 Å (for example, 1.67 ± 0.05 Å in B_2F_4;[31] 1.70 ± 0.04 Å in B_2Cl_4;[32,33] 1.698 and 1.711 Å in B_2H_4;[34–36] 1.74 Å between two apical boron atoms in

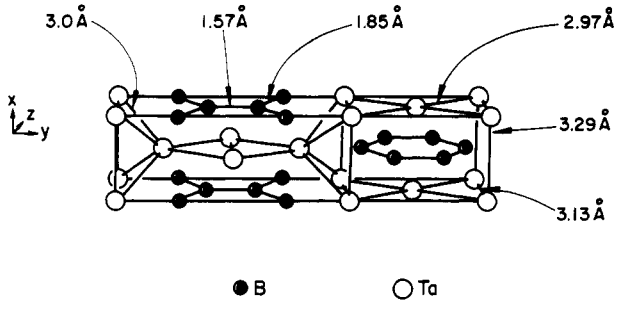

2

(26) (a) Hoffmann, R. *J. Chem. Phys.* **1963**, *39*, 1397. (b) Hoffmann, R.; Lipscomb, W. N. *J. Chem. Phys.* **1962**, *36*, 2179, 3489; **1962**, *37*, 2872. (c) Ammeter, J. H.; Burgi, H.-B.; Thibeaut, J. C.; Hoffmann, R. *J. Am. Chem. Soc.* **1978**, *100*, 3686. (d) Whangbo, M.-H.; Hoffmann, R. *J. Am. Chem. Soc.* **1978**, *100*, 6093.

(27) (a) Fenske, R. F. *Pure Appl. Chem.* **1988**, *60*, 1153. (b) Blyholder, G.; Coulson, C. A. *Theor. Chim. Acta* **1968**, *10*, 316. (c) Anderson, A. B.; Hoffmann, R. *J. Chem. Phys.* **1974**, *60*, 4271. (d) Anderson, A. B. *J. Chem. Phys.* **1975**, *62*, 1187. (e) Wooley, R. G. *Nouv. J. Chem.* **1981**, *5*, 219, 227.

(28) (a) Kiessling, R. *Acta Chem. Scand.* **1949**, *3*, 603. (b) Kiessling, R. *Acta Chem. Scand.* **1950**, *4*, 209. (c) Elfström, M. *Acta Chem. Scand.* **1961**, *15*, 1178. (d) Kiessling, R. *Acta Chem. Scand.* **1950**, *4*, 146.

(29) *International Tables for Crystallography*; Hahn, A., Ed.; D. Reidel: Company, Boston, **1983**; Vol. A.

(30) Fenish, R. G. *Trans. Metallurg. Soc.* AIME **1966**, *236*, 804.

(31) Trefonas, L.; Lipscomb, W. N. *J. Chem. Phys.* **1958**, *28*, 54.

(32) Atoji, M.; Lipscomb, W. N. *Acta Crystallogr.* **1953**, *6*, 547.

(33) Ryan, R. R.; Hedberg, K. *J. Chem. Phys.* **1969**, *50*, 4986.

(34) Houbold, W.; Hrebicek, J.; Sawitzki, G. Z. *Naturforsch., B: Anorg. Chem., Org. Chem.* **1984**, *39B*, 1027.

(35) Nöth, H. Z. *Naturforsch, B: Anorg. Chem., Org. Chem.* **1984**, *39B*, 1463.

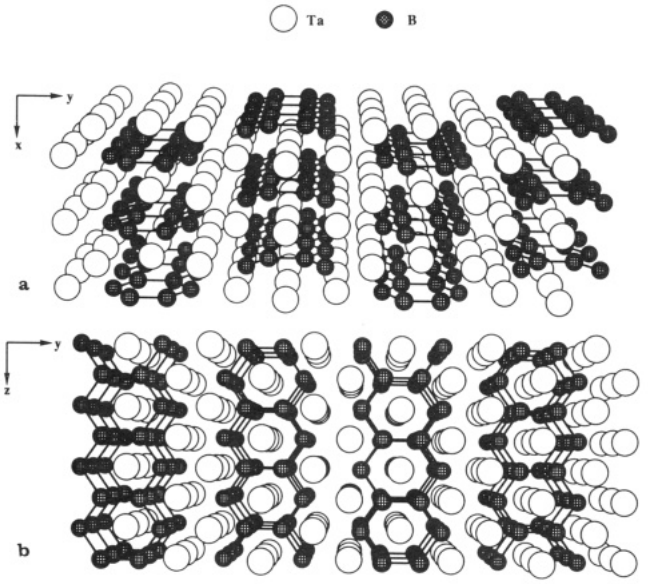

Figure 1. Two perspective views of the Ta_3B_4 crystal structure: (a) seen along the x axis, (b) along the z axis.

$B_{10}H_{16}$).[37] B=B double bonds are rare. They have been assumed to exist only in the cation B_2Cl^{2+}, observed in the mass spectral fragmentation of B_2Cl_4,[38] and in the dication B_2^{2+} generated in a tandem accelerator.[39] There is no good estimate of a B=B double bond distance, as far as we know.

Two perspective views of the Ta_3B_4 structure are shown in Figure 1. The one-dimensional polyacene-type chains of the boron sublattice are apparent. Polyacene (C_4H_2) itself is an organic polymer of some interest,[40] and similar main-group chains occur in the AlSi sublattice of $Ca_3Al_2Si_2$.[41,42] The electron counts are very different for all of these, yet there is a striking geometrical relationship among them that we must explore. We begin with the boron sublattice.

The Boron Chain

Figure 1 suggests that the polyacene-type boron chains are relatively isolated from each other (but not from the Ta sublattice). We probed this by examining one-, two-, and three-dimensional boron-only pieces of the full structure. The one-dimensional chain is **3**, the two-dimensional array a stack of these on top of each other (i.e., a vertical slice through Figure 1a), the three-dimensional model the full boron sublattice of Ta_3B_4. The band structures shown in Figure 2 are very similar, and the out-of-plane dispersion of the isolated three-dimensional boron sublattice in the Ta_3B_4 is small. So in the sequel we restrict ourselves to the one-dimensional chain.

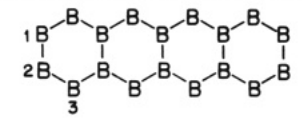

3

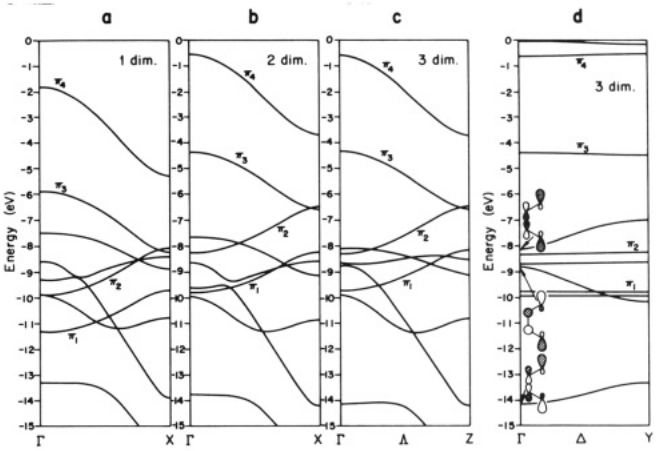

Figure 2. Band structure of the $(B_4)_\infty$ chain in Ta_3B_4 in (a) one; (b) two, (c) and (d) three dimensions. In (b) and (c) the band dispersion along the chain axis is shown, for comparison with (a). In (d) is shown the dispersion perpendicular to the chain axis.

We next symmetrized the boron chain, making all B–B 1.76 Å. If one is searching for the explanation of a bond-length differential, it is useful to construct a hypothetical more symmetric system, with the relevant bond lengths equal. Then one can look into the electronic structure, especially the overlap population, for the origin of the differentiation.[43-48] The bonding characteristics of the one-dimensional chain are shown in Figure 3. They are very similar to those of the symmetrized chain (compare Figures 2a and 3a).

To explain the band structure in more detail, we begin with the construction of the MOs for the B_4 unit. The construction principle we should like to follow is **4** → **5** → **6**. These steps are accomplished in Figure 4.

4

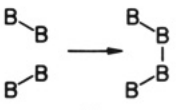

5

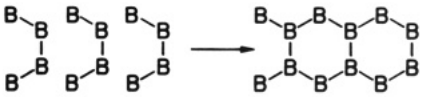

6

The shape and the order of the B_2 MOs are quite similar to those of any main-group diatomic molecule.[42,49] In the second step the MOs of the B_4 unit cell are formed. It is

(36) Mohr, R. R.; Lipscomb, W. N. *Inorg. Chem.* **1986**, *25*, 1053.
(37) Grimes, R. N.; Wang, F. E.; Lewin, R.; Lipscomb, W. N. *Proc. Natl. Acad. Sci. U.S.A.* **1961**, *47*, 996.
(38) Dibeler, V. H.; Walker, J. A. *Inorg. Chem.* **1969**, *8*, 50.
(39) Galindo-Uribarri, A.; Lee, H. W.; Chang, K. H. *J. Chem. Phys.* **1985**, *83*, 3685.
(40) (a) Whangbo, M.-H.; Hoffmann, R.; Woodward, R. B. *Proc. R. Soc. London.* **1979**, *A366*, 23. (b) Kertesz, M.; Hoffmann, R. *Solid State Commun.* **1983**, *47*, 97. (c) Whangbo, M.-H. In *Crystal Chemistry and Properties of Materials with Quasi-One-Dimensional Structures*; Rouxel, J., Ed.; Reidel: Dordrecht, Holland, 1986; pp 27–85.
(41) Widera, A.; Schäfer, H. Z. *Naturforsch. B.* **1977**, *32B*, 1349.
(42) Li, J.; Hoffmann, R. *J. Phys. Chem.* **1988**, *92*, 887.
(43) Jahn, H. A.; Teller, E. *Proc. R. Soc. London* **1937**, *A161*, 220.
(44) Pearson, R. G. *Symmetry Rules for Chemical Reactions*; Wiley: New York, 1976.
(45) (a) Burdett, J. K.; *Molecular Shapes*; Wiley: New York, 1980. (b) Bersuker, I. B.; *The Jahn–Teller Effect and Vibronic Interaction in Modern Chemistry*; Plenum Press: New York, 1984. (c) Bersuker, I. B.; Polinger, V. Z. *Vibronic Interaction in Molecules and Crystals*; Springer-Verlag, New York, 1989.
(46) Peierls, R. E. *Quantum Theory of Solids*; Oxford University Press: Oxford, 1972.
(47) Hoffmann, R. *Solids and Surfaces: A Chemist's View of Bonding in Extended Structures*; VCH Publishers: New York, 1988.
(48) Burdett, J. K. *Prog. Solid. State Chem.* **1984**, *15*, 173.
(49) Gimarc, B. M. *Molecular Structure and Bonding: The Qualitative Molecular Orbital Approach*; Academic Press: New York, 1979.

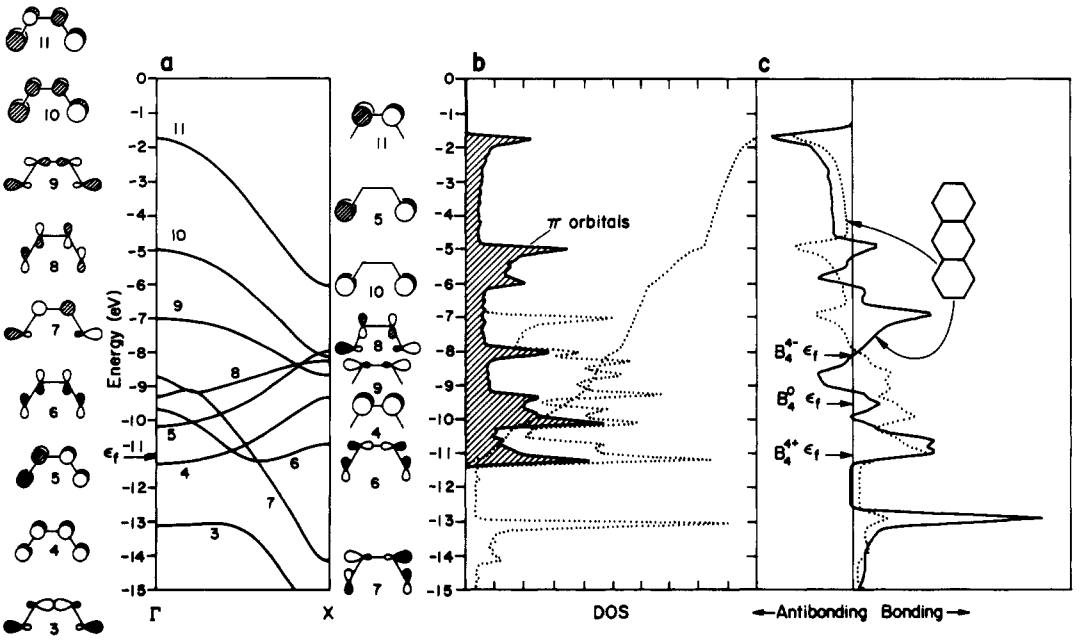

Figure 3. Band structure and DOS and COOP curves for the one-dimensional $(B_4)_\infty$ chain with equal B–B bonds: (a) band structure; (b) DOS curves. The contribution of all π orbitals of the boron chain is shown by the shaded area in the middle panel; the dashed line is the total DOS, the dotted line an integration of the π contribution. (c) COOP curves of the two B–B bonds. In this case three positions of the Fermi level are shown, for $(B_4)^{4+}_\infty$, $(B_4)^{0}_\infty$, and $(B_4)^{4-}_\infty$ chains.

apparent from 6 that the degeneracies of the π-orbitals are removed. The shape and the order of the B_4 MOs are also the same as in C_4 and other main-group A_4 molecules with similar geometric configurations.[49]

Consequently, as derived in Figure 6 and by analogy with polyacene,[42] we expect four π-bands, as indicated in 7. These are bands 4, 5, 10, and 11 in Figure 3. We might

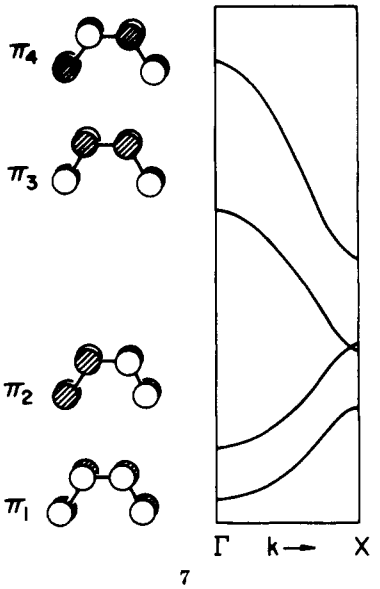

7

also expect two high-lying boron lone pair bands, as shown schematically in 8. These in fact mix with other σ bands

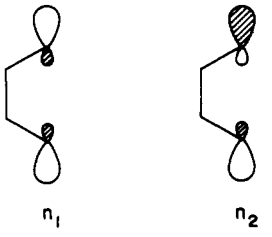

8

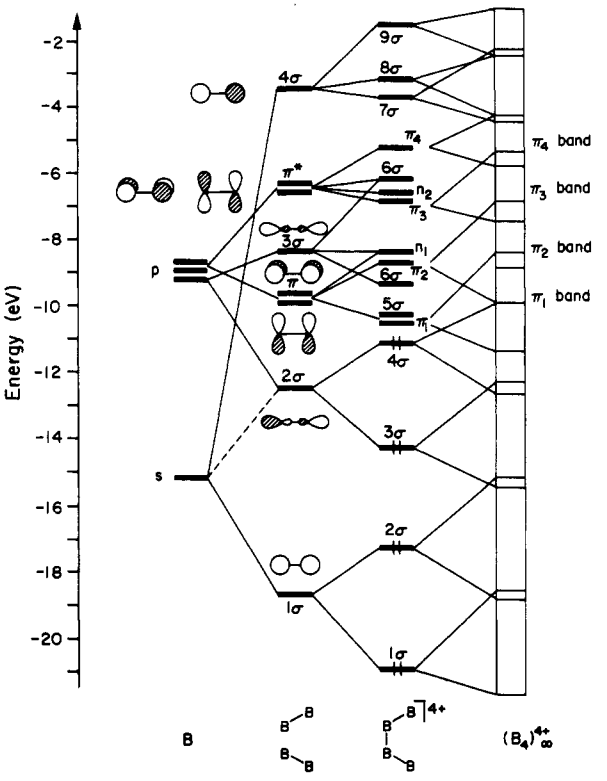

Figure 4. Schematic diagram showing the orbital interactions, when, first, two borons are brought together to form the diatomic B_2 then, second, two B_2 units form a "*cis*-butadiene" B_4 structure, and, finally B_4 units link together to form the $(B_2)_\infty$ chain.

but may be identified as bands 7 and 9 in Figure 3. Note that these σ bands come quite high in energy, band no. 9 being in the same region of energy as the third π level.

Before we decide what bonding to expect from such a chain, we must worry about the electron count. What is the charge on the polyacene B chain in the full Ta_3B_4 structure? Anticipating a result we will discuss in detail below, we find 3.1 electrons/Ta_3B_4 formula unit transferred from B_4 to Ta_3 in the three-dimensional structure, i.e., a

positive B_4 chain. For a neutral one-dimensional chain the Fermi level would be at -9.61 eV and for a $(B_4)^{4+}$ chain at -11.09 eV. These fillings are marked by arrows in Figure 3. Note that the region depopulated on going from $(B_4)^0$ to $(B_4)^{4+}$ is both B_1–B_2 and B_2–B_3 bonding. This is indicated in another way in **9**. The bands in question (-9.5

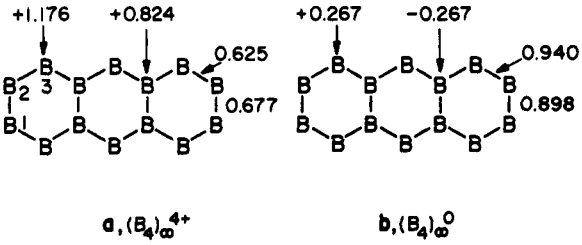

9

to -11 eV) are 4, 5, 6 and 7 (at Γ), both π and σ, so it is difficult to trace any differentiation to one or another bond type. The net overlap populations, shown in **9**, clearly indicate that both B–B bonds are weakened on oxidation but that B_1–B_2 emerges stronger.

The charge distribution in **9a** and **9b** shows that the three-coordinate boron possesses a larger electron density than the two-coordinate one. Knowledge of the site with the highest electron density is important for evaluating substituents effects. The more electronegative substituent will preferentially enter a site with greater electron density, in accord with the rule of topological charge stabilization.[48,50]

Next we studied the stability of the boron chain by itself, specifically with respect to distortions leading from the symmetrized (all B–B 1.76 Å) to the real, unsymmetric (B–B 1.57 and 1.85 Å) structure. For B_4^{4+} and every dimensionality the incorrect symmetrized structure is preferred. This is a hint that Ta–B interactions are critical in the energetics of the full structure, a point to which we will soon return.

The Ta Sublattice

The tantalum sublattice in Ta_3B_4 contains two kinds of metal atoms, Ta_1 and Ta_2 (see **1**, **2**, and **10**). Atom Ta_2,

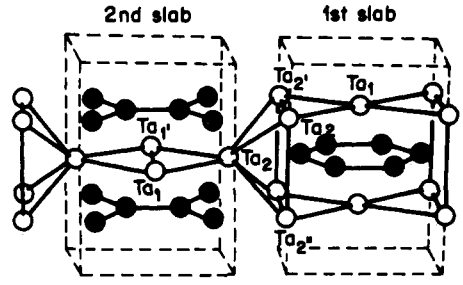

10

located in the 4(g) position,[28a,29] has six nearest neighbors, two at 2.97 Å and four at 3.00 Å. Ta_1 lies in the 2(c) position, surrounded by four metal neighbors at 2.97 Å, two at 3.13 Å, and two at 3.29 Å.[28a] We can compare these distances with the Ta–Ta separations in the crystal structure of pure tantalum. The metal has a body-centered cubic structure with a = 3.3029 Å at room temperature (291 K).[51] The shortest distance between atoms in this structure is 2.86 Å. So all metal–metal distances in the Ta_3B_4 structure are somewhat longer than in metallic Ta.

Whereas the boron sublattice in Ta_3B_4 shows one-dimensional features, that is not so for the Ta sublattice. One-dimensional models miss four Ta_2–Ta_2, interactions, all at short distances. So do two-dimensional slabs. Computations on low-dimensional models confirm this. Only the full three-dimensional sublattice of Ta_3B_4 captures the full range of Ta–Ta interactions.

It also turns out that the three-dimensional $(Ta_3)^{3-}$ sublattice is less stable in the "real" structure than a hypothetical symmetrized one, emphasizing again the importance of B–Ta interactions. This we will discuss in the next section.

The Full Ta_3B_4 Structure

The band structure of Ta_3B_4 and the associated DOS are shown in Figure 5. The Fermi level crosses several bands; we expect this material to be metallic. This is in accord with experimental data.[1-3]

Note the most obvious feature of the Ta_3B_4 DOS—the boron and tantalum states are not segregated but are mixed over a wide range of energies. Obviously the band structure of Ta_3B_4 is not simple. Could it be that in this complexity are contained electronic features of substructures of lower dimensionality, in particular the polyacene-like boron sublattice that we noted?

We probed this point by constructing such sublattices and comparing the band structures. This was done in the context of a "symmetrized" model with equal Ta–Ta bonds in the tantalum chain and B–B bonds in the boron chain. The Ta–Ta bond lengths are chosen as 3.05 Å. This value is the average of the two different Ta–Ta bond lengths (3.13 and 2.97 Å) in the one-dimensional cut of the full crystal structure. The B–B bond lengths defined by the Ta–Ta distance chosen are then 1.76 Å. The distance between the planes containing boron or tantalum chains is also changed a little, in order for the volume of the unit cell (V = 144 Å^3) to remain the same.

A "zero-dimensional" model might be the discrete Ta_3B_4 molecule of the unit cell, **11**. One obvious one-dimensional

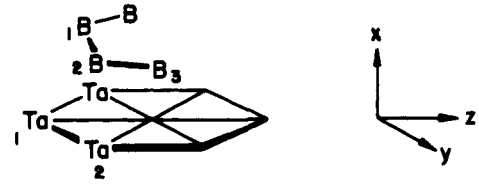

11

sublattice is the isolated boron chain, shown in a "top" view, **3**. Another one is a pair of B and Ta chains, **12**, and a third a pair of tantalum chains sandwiching the B polyacene chain, **13**.

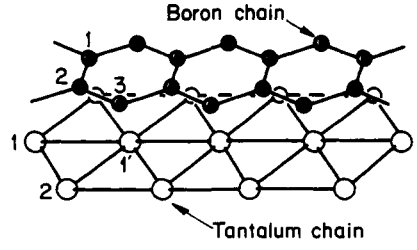

12

An obvious two-dimensional sublattice is a stack of alternating Ta and B chains, **14**.

(50) Gimarc, B. M. *J. Am. Chem. Soc.* **1983**, *105*, 1979.
(51) (a) Edwards, J. W.; Speiser, R.; Johnson, H. L. *J. Appl. Phys.* **1951**, *22*, 424. (b) Iga, A.; Tawara, Y. *J. Phys. Soc. Jpn.* **1968**, *24*, 28.

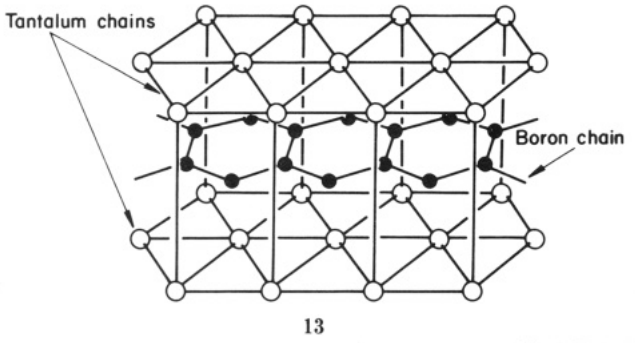

13

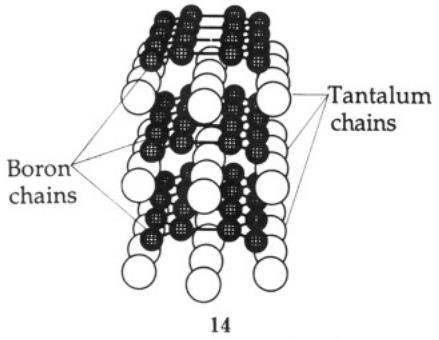

14

The evolution of the DOS curves for the Ta_3B_4 structures as one moves from zero through one, two, and on to three dimensions is presented in Figure 6.

The DOS curves are changed drastically at each step. Note in particular that when we go from two- to three-dimensional models, two peaks appear in the total DOS curve. These are derived mainly from the d AOs of the tantalum sublattice (see Figure 6). The contribution of the boron orbitals to the total DOS in this region is comparatively small and is gradually distributed over a broad range of energies, with small peaks in the region of the d AO Ta peaks. The strong changes in the DOS as a function of dimensionality argue again that the Ta_3B_4 structure is essentially three-dimensional.

The relative energetic stability of the real and hypothetical symmetrized Ta_3B_4 crystal structures in zero-, one-, two-, and three-dimensional substructures is presented in Table III. In all cases we see that the symmetrized structure is less stable than the real structure. The two forms have consistently similar Fermi levels. Also the Fermi levels nearly do not change as one proceeds from zero, through one, to two dimensions. However, on moving to three dimensions, the Fermi level rises abruptly. A new interaction is turned on, between Ta–Ta and B–Ta atoms belonging to neighboring slabs in the Ta_3B_4 three-dimensional crystal structure. It is clear again that Ta_3B_4 is inherently three-dimensional, as far as its electronic structures is concerned.

That the hypothetical "bond-length-symmetrized" model Ta_3B_4 structure is less stable than the real one is as it should be. Recall that when we looked at the isolated Ta and B sublattices, this was not true, i.e., the symmetrical structure was incorrectly calculated to be more stable.

The overlap populations of the B–B and Ta–Ta bonds in the symmetrized models are presented in Table IV. We can see that in cases of one, two and three dimensions the B_1–B_2 bond has a substantially larger overlap population than the B_2–B_3 bond. Also the overlap population of the Ta_1–Ta_2 bond is larger than that the Ta_1–$Ta_{1'}$ bond. These differences in overlap populations are consistent with the observed deformations in the real structure.

What about the electron distribution in Ta_3B_4? We calculate 3.1 electrons transferred from B_4 to Ta_3, i.e., $[Ta_3]^{3.1-}[B_4]^{3.1+}$.

Table III. Relative Energy (ΔE) per Unit Cell and Fermi Level (ϵ_f) for the Real and Symmetrized Sections of the Ta_3B_4 Crystal Structure

dimensionality	structure		ΔE, eV	ϵ_f, eV
0	11	symmetrized	0.62	−11.75
		real	[0]	−11.67
1[a]	12 (13)	symmetrized	0.36 (0.39)	−11.50 (−11.80)
		real	[0]	−11.57 (−11.85)
2	14	symmetrized	0.3	−11.31
		real	[0]	−11.32
3		symmetrized	0.10	−10.37
		real	[0]	−10.28

[a] In the one-dimensional case we used two models: first, one tantalum chain and one boron chain above (12); second, two parallel tantalum chains with a boron chain between them (13, the numbers in parentheses).

Table IV. Overlap Population of the B–B and Ta–Ta Bonds in the Symmetrized Hypothetical Ta_3B_4 Structure, Compared to Observed Bond Lengths

bond	overlap population	bond lengths in Ta_3B_4, Å
B_1–B_2	0.437	1.57
B_2–B_3	0.378	1.85
Ta_1–$Ta_{1'}$	0.177	3.13
Ta_1–Ta_2	0.214	2.97

Charge transfer between two sublattices is a fundamental characteristic of their interaction and, consequently, bonding. In principle, two directions of charge transfer between boron and metal sublattices are possible in the TMB. Calculations[14] of the electronic structure of the TMB with an AlB_2 structure show that the charge on the boron depends on the d electron count of the metal atom M. The boron charge changes from +0.8 to −0.4 in the series M = Ca, Sc, Ti, V, Cr, Fe, Co, and Ni. The crossover is near iron. Calculations[24] on the MB_4 TMB with M = V, Cr, Mn, Fe, and Co yield a charge on boron of +0.47, +0.37, +0.28, +0.12, and −0.06, respectively. At the same time, calculations on TiB_2[23] and MB borides with M = Ti, Mn, Fe, and Co[22] show the opposite direction of charge transfer—from metal to boron. Experimental work[49] on the magnetic and electrical properties of sub- and monoborides of transition metals shows that every boron atom yields approximately 1.7–1.8 electrons to the metal d-band. The same conclusion concerning charge transfer from boron to metal may be made on the basis of Mössbauer[50] and X-ray spectra[51] and from studies of the low-temperature specific heat.[52]

The experimental data thus confirm our calculated direction of charge transfer, which is contrary to the electronegativity of boron and metals[13] (concerning the electronegativity of the elements, see the recent work of Allen).[53] A way to think about this is that the the direction of charge transfer in an extended material, e.g., Ta_3B_4, is defined by the position of the Fermi levels of the boron and tantalum sublattices rather than the energies of isolated atoms. Our calculations show that the values of the Fermi level of the three-dimensional boron and tantalum sublattices are equal to −9.31 (B) and −12.63 eV (Ta), respectively. As one can see from Table III, the value of the Fermi level in the Ta_3B_4 structure is near the average

(52) Cadeville, M. C.; Daniel, E. *J. Phys. (Paris)* **1966**, *27*, 449.
(53) Cooper, J. D.; Gib, T. C.; Greenwood, N. N.; Parish, R. V. *Trans. Faraday Soc.* **1964**, *60*, 2097.
(54) Zhurakovskii, E. A.; Kotlyar, V. I.; Shashkina, T. B. *Dopov. Acad. Nauk Ukr. RSR, Ser. A* **1969**, No. 7, 12.
(55) Tyan, Y. S.; Toth, L. E.; Chang, Y. A. *J. Phys. Chem. Solids*, **1969**, *30*, 785.
(56) Allen, L. C. *J. Am. Chem. Soc.* **1989**, *111*, 9003.

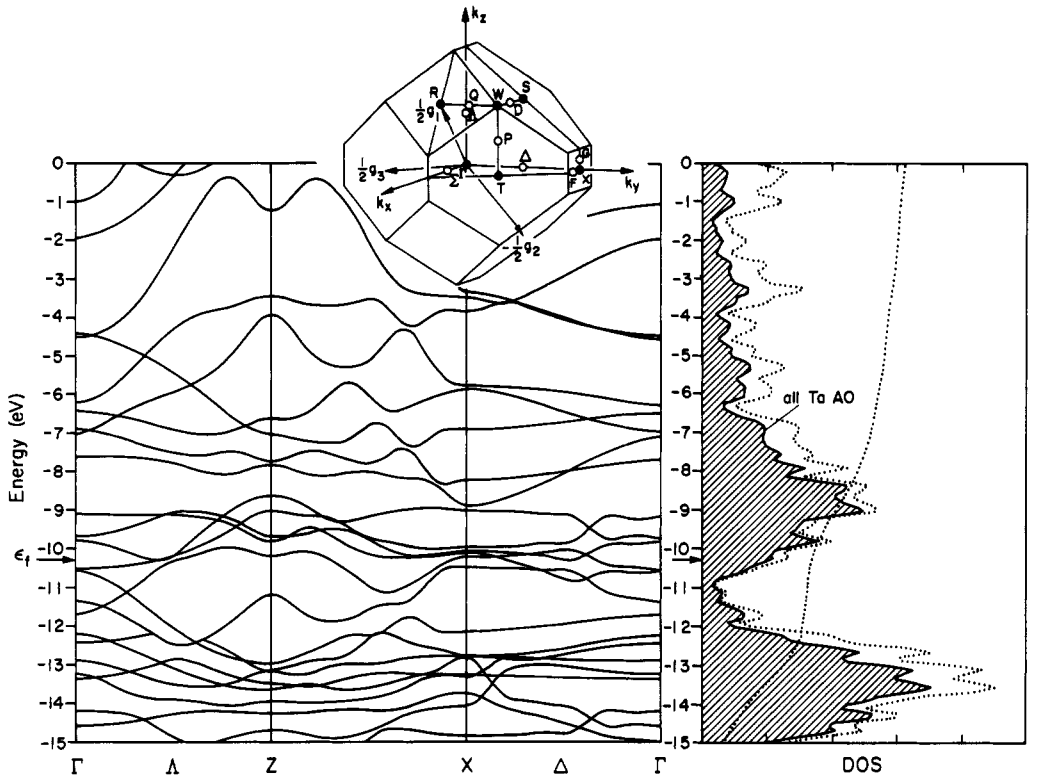

Figure 5. Band structure and DOS of the Ta_3B_4 lattice. The contributions of all tantalum AOs are shown by the shaded area in the right panel. The dotted line in the right panel gives integration of the projected DOS.

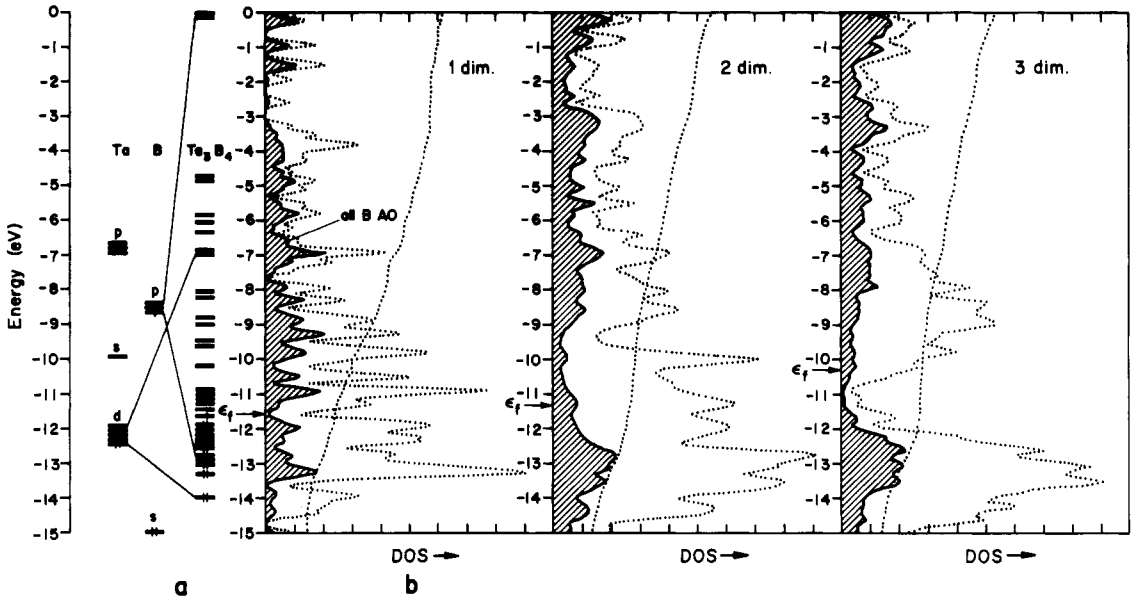

Figure 6. Evolution of DOS curves of the Ta_3B_4 structure in the series: (a) zero-dimensional, molecule 11; (b) one- (12), (c) two- (14), and (d) three-dimensional full structure (see Figure 1). The shaded areas show the contribution of all boron AOs.

Table V. Binding Energy per Unit Cell as a Function of the d-Electron Count (n) for the TMB with the Ta_3B_4 Structure

d^n	first element of triad	binding energy, eV	d^n	first element of triad	binding energy, eV
1	Sc	111.6	6	Fe	56.2
2	Ti	114.7	7	Co	29.1
3	V	111.4	8	Ni	-5.0
4	Cr	97.6	9	Cu	-38.2
5	Mn	78.7	10	Zn	-81.7

of the boron and tantalum sublattices. Consequently, to align the Fermi levels in both boron and metal substructures, some electron density flows from boron to tantalum sublattices. This situation is illustrated schematically by **15**.

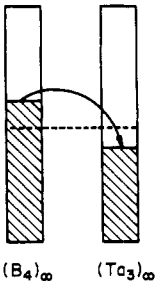

15

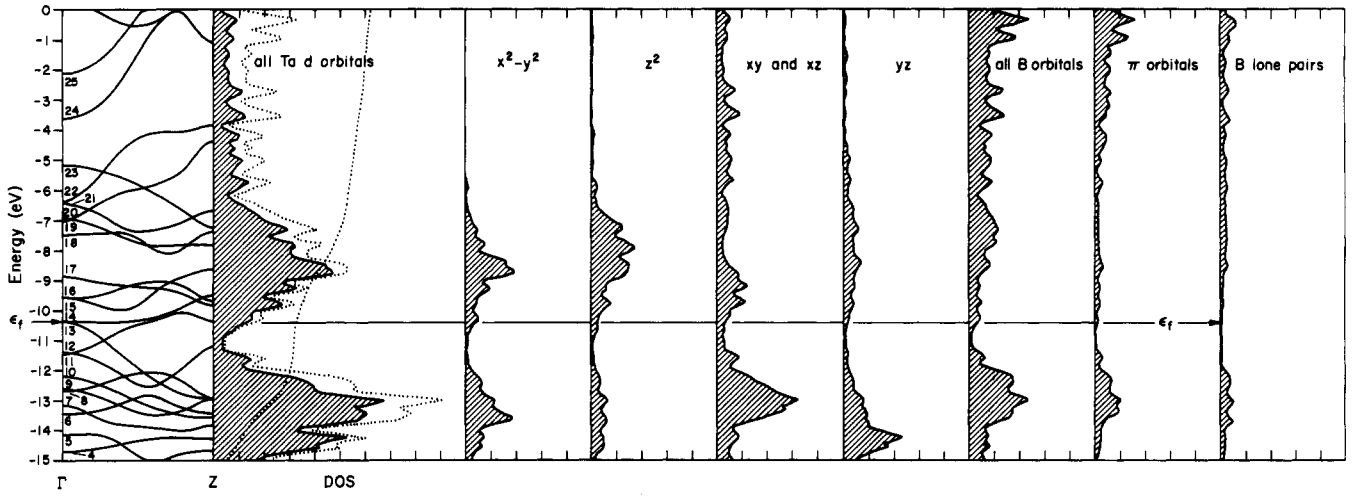

Figure 7. (a) Band structure and DOS calculated for the three-dimensional hypothetical symmetrized Ta_3B_4 structure. Lined regions designate the DOS projected for different orbitals: (b) d AO's of all tantalum atoms; (c) $d_{x^2-y^2}$; (d) d_{z^2}; (e) d_{xy} and d_{xz}; (f) d_{yz}; (g) all boron orbitals; (h) π orbitals; (i) p_y (lone pair) of boron chain.

Interaction of Tantalum and Boron Sublattices and Stability of the Ta_3B_4 Structure

The argument for the importance of Ta–B interaction is pretty clear: separate B and Ta sublattices of every dimensionality favor a symmetrized, unrealistic structure, whereas B–Ta bonded sublattices consistently prefer the real, unsymmetric geometry (see Table III).

In Figure 7 we show the band structure calculated along Λ, and the total DOS with its decomposition into contributions from tantalum d atomic orbitals (AOs) and boron s,p orbitals, for the hypothetical symmetrized Ta_3B_4 crystal structure. The main contribution to the low-energy peak of the total DOS comes from the d AOs of tantalum atoms. In turn, the greatest contribution to that low-energy peak comes from the $d_{x^2-y^2}$, d_{xy}, d_{xz}, and d_{yz} tantalum orbitals.

From Figure 7 we notice that the main contribution to the low-energy peak of the d_{yz} projection derives from band 4. The orbital composition of this band at Γ and Z is shown in **16**. The low energy peak of the tantalum d_{xy},

16

17

d_{xz}, and boron π projections derives from band 7 (shown in **17**). The upper peak on the total DOS curve consists mainly of $d_{x^2-y^2}$ and d_{z^2} tantalum orbitals.

There are two different interactions between atoms in the two sublattices: first, those between orbitals of boron chains and d AOs of tantalum atoms perpendicular to chain plane direction, and second, interaction between orbitals of boron atoms located at 2-fold sites and orbitals of the corner Ta_2 (see **1**, **2**, and **10**) atoms belonging to neighboring slabs.

To trace the main orbital interactions that stabilize the crystal structure, one might construct an appropriate

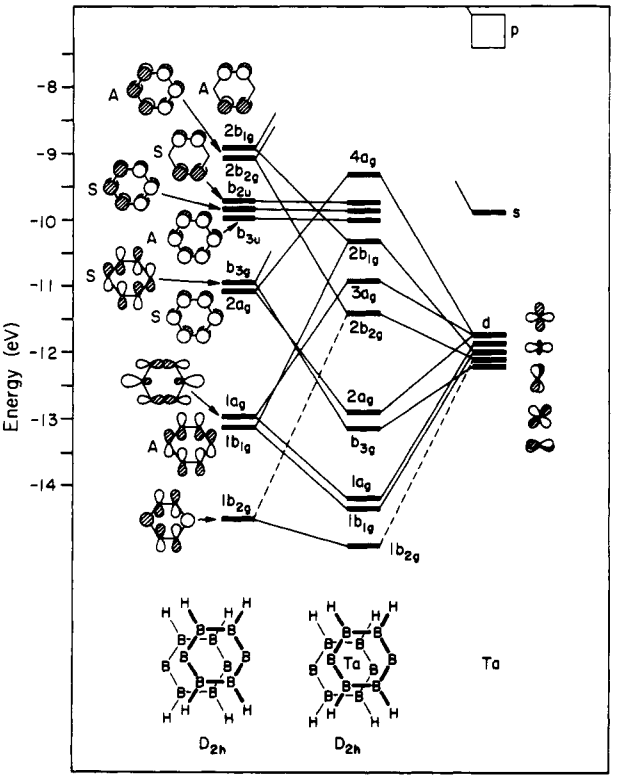

Figure 8. Molecular orbital interaction diagram for $(B_6H_4)Ta$, **18**. As we show the shape of the MO only for the upper ring, we introduce the latters A and S to denote the symmetry of the MO with respect to the mirror plane. Dashed lines designate small contributions of fragment MOs.

molecular model. This is not easy, for if we try to replace the Ta_3B_4 crystal structure by some small molecule, we invariably lose some important part of the intracrystal interaction. To simulate the interaction in the direction perpendicular to the boron and tantalum chains, we choose the sandwich structure **18**. For modeling lateral interslab

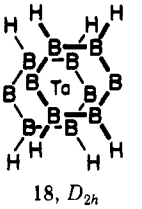

18, D_{2h}

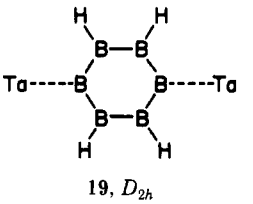

19, D_{2h}

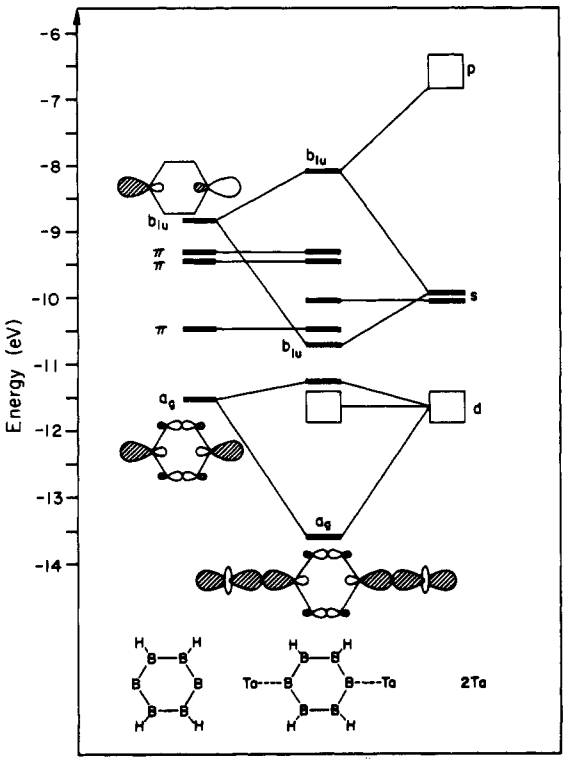

Figure 9. Molecular orbital interaction diagram for model **19**.

interaction between boron and tantalum orbitals, we have calculated the model **19**. In Figure 8 we show the interaction diagram for the structure **18**.

The main stabilizing interaction is between σ $1b_{1g}$, $1a_g$, and b_{3g} MOs of boron rings with d AOs of tantalum atom. All π orbitals, except the lowest $2a_g$ MO, do not take part in interaction with the d AOs of the metal atom. Hence in our case the main interactions that stabilize the sandwich molecule, **18**, are those of σ MOs of the boron rings with d AOs of the central metal atom. Thus $(H_4B_6)_2Ta$ contrasts with chromocene[57] and ferrocene,[58] where the main stabilizing interaction is that of the e_{1g} benzene π orbital with the metal e_{1g} (d_{xz} and d_{yz}) orbitals.

For model **19**, the main interaction that stabilizes the system is the σ interaction between boron lone pairs and the d_{z^2} of the tantalum atoms. The orbital interaction diagram for **19** is depicted in Figure 9.

It is instructive to compare the hypothetical sandwich compound $(B_6H_4)_2Ta$, **18**, and also the more symmetrical $(B_6H_6)_2Ta$ with known metalloboranes.

The history of the transition metal complexes of boron-containing ring ligands is relatively recent, beginning in 1965,[59] when the first metallocarboranes were synthesized. These metallocarboranes,[60] incorporating most of the transition metals, are of the types $[(C_2B_4H_{11})_2M]^{n-}$, **20**, $[(C_2B_9H_{11})M(C_5H_5)]^{m-}$, **21**, or $[(C_2B_9H_{11})_2M]^{k-}$, **22**, in

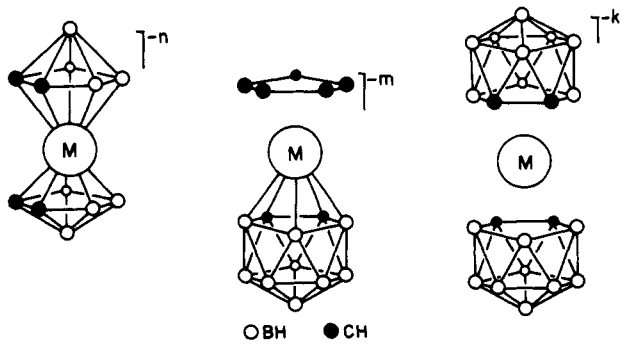

20 **21** **22**

which the $C_2B_4H_{11}$ or $C_2B_9H_{11}^{2-}$ ligands replace $C_5H_5^-$. It is interesting to note that many metallocarboranes are more stable than their metallocene counterparts.[59,60] We note here the carborane polymers **23**, synthesized by Sie-

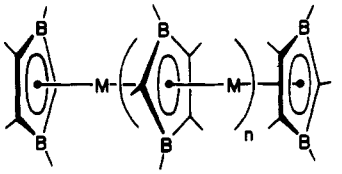

23, M = Ni, Rh

bert and co-workers.[59d-f] An obvious structural extension of these compounds is to polymeric chains **24** (where X is a main-group element). Such compounds provide, in principle, rich possibilities for variation of electron count to stabilize double- (n = 0) and triple-decker (n = 1) and perhaps polymeric (n = ∞) metalloboron compounds.

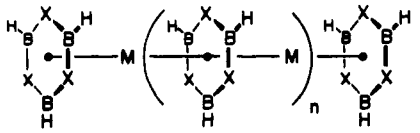

24

Let us discuss the stability of the M_3B_4 borides as a function of the metal d electron count. In Table V we list the binding energies per unit cell, defined as E(separated atoms) – E_{total}, of the TMB with Ta_3B_4 structure. We see the binding energy decreases with increasing n, so that by the time one reaches the d^8 elements the binding energy becomes negative. Consequently TMB compounds with a Ta_3B_4 crystal structure d^8–d^{10} transition metals should be unstable. Also the stability of M_3B_4 with d^6–d^7 elements is less than that for other TMB. The behavior of the binding energy as a function of n explains the stability trend observed in Table I. But where does this trend come from?

The place to seek energetic preferences is in the bonding. And one could also attempt to go back from the Ta_3B_4 structure to the one-dimensional B_4 chain discussed in a previous section. Figure 10 shows the B–B COOP curves for the B_4 chain and the full Ta_3B_4 structure. Assuming a rigid-band model, we also show how different electron counts would fill these bands.

Note, first of all, similiarities in the one-dimensional boron sublattice and the three-dimensional Ta_3B_4 COOP, especially in the lower energy region. On moving up in electron count from Ta_3B_4, the B_2–B_3 bond should strengthen.

In the region of electron occupations corresponding to most transition metals the COOP curves of the two B–B bonds show bonding (see Figure 3c). Consequently the overlap population of these bonds should rise with increasing electron count, and this is shown in another way

(57) Burdett, J. K.; Canadell, E. *Organometallics* **1985**, *4*, 805.
(58) Albright, T. A.; Burdett, J. K.; Whangbo, M.-H. *Orbital Interactions in Chemistry*; Wiley: New York, 1985.
(59) (a) Hawthorne, M. F.; Young, D. C.; Wegner, P. A. *J. Am. Chem. Soc.* **1965**, *87*, 1818. (b) Hawthorne, M. F. *J. Organomet. Chem.* **1975**, *100*, 97. (c) Callahan, K. P.; Hawthorne, M. F. *Adv. Organomet. Chem.* **1976**, *14*, 945. (d) Siebert, W. *Pure Appl. Chem.* **1988**, *60*, 1345. (e) Siebert, W. *Angew. Chem., Int. Ed. Engl.* **1985**, *24*, 943. (f) Knörzer, G.; Siebert, W. *Z. Naturforsch. B* **1990**, *45*, 15.
(60) (a) Dunks, G. B.; Hawthorne, M. F. In *Boron Hydrite Chemistry*; Muetterties, E. L., Ed.; Acadenic Press: New York, 1975. (b) Grimes, R. N. *Acc. Chem. Res.* **1978**, *11*, 420. (c) Grimes, R. N. *Coord. Chem. Rev.* **1979**, *28*, 47. (d) Grimes, R. N. In *Comprehensive Organometallic Chemistry*; Wilkinson, G., Ed.; Pergamon Press: New York, 1982; Vol. 1. (e) Mingos, D. M. P. In *Comprehensive Organometallic Chemistry*; Wilkinson, G., Ed.; Pergamon Press: New York, 1982; Vol. 3.

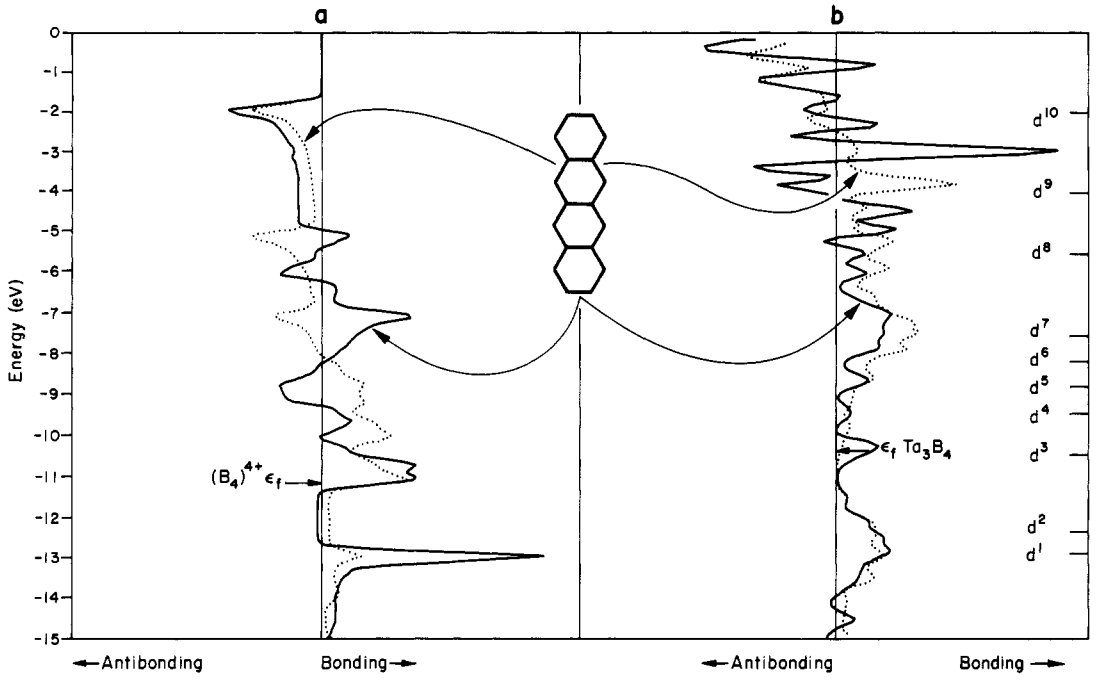

Figure 10. COOP curves of the two B–B bonds: (a) in the one-dimensional boron chains with equal bonds; (b) in the boron sublattice of the three-dimensional symmetrized Ta_3B_4 structure. The position of the Fermi level for d^n (n = 1–10) metals is shown by a bar in the right panel.

in Figure 11. There is an interesting crossover in the theoretical strength of the two distinct B–B bonds between d^6 and d^7.

A greater overlap population should lead to strengthened and shortened B–B bonds. Indeed from Table II one can see that there is such a tendency, i.e., decreasing B–B bond lengths in the series Ta, Cr, and Mn. The crossover between B_1–B_2 and B_2–B_3 bonds is observed in some known ternary TMB with the Ta_3B_4 crystal structure. For example the boride Ru_2MoB_4[61] has B_1–B_2 and B_2–B_3 bond lengths equal to 1.80 and 1.72 Å, respectively. The same order is observed in the $MoFe_2B_4$ structure.[62]

The way the overlap populations of different bonds in hypothetical symmetrized Ta_3B_4 structures depend on d-electron count is shown in Figure 12.

We see that the values of the overlap population of bonds 9 and 10 (the designation of various bonds in the Ta_3B_4 unit cell is given in **25**) do not differ strongly from

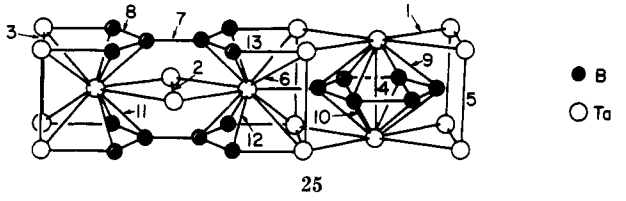

25

the values 0.294 and 0.233, respectively, for the Ta–B bond overlap populations in **18**.

As these overlap populations (or corresponding COOPs, not shown here) indicate, the metal–metal OPs become antibonding around d^5. In the region of d^5–d^{10} electron counts the total overlap population for these bonds is decreasing. The optimal stability region for M_3B_4 compounds with the Ta_3B_4 crystal structure occurs for d^1–d^5 metals. M_3B_4 compounds with d^6–d^{10} metals should be unstable. We think that is the main reason these com-

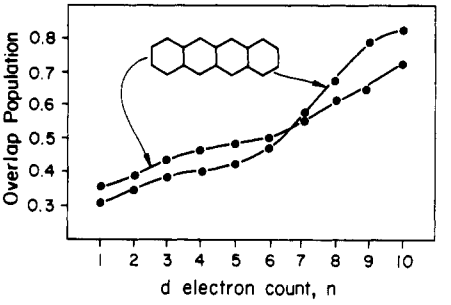

Figure 11. Dependence of the overlap population of the two B–B bonds on d-electron count in the boron chain for the transition-metal borides with the Ta_3B_4 crystal structure.

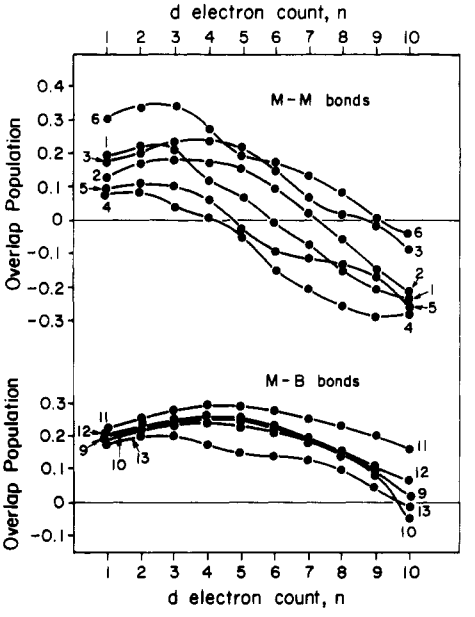

Figure 12. Dependence of overlap population for M–M and M–B bonds on d-electron count in transition metal borides M_3B_4 with the Ta_3B_4 crystal structure. The curves are numbered as in structure **25**.

(61) Rögl, P.; Benesovsky, F.; Nowotny, H. *Monatsh. Chem.* **1972**, *B103*, 965.

(62) Gladischevskii, E. I.; Fedorow, T. F.; Kuz'ma, Yu. B.; Skolosdra, R. W. *Poroshk. Metall.* **1966**, *4*, 55.

Table VI. Atomic Parameters Used in the Calculations

atom	orbital	H_{ii}, eV	ζ_1	ζ_2	c_1[a]	c_2[a]
H	1s	-13.60	1.30			
B	2s	-15.20	1.30			
	2p	-8.50	1.30			
Ta	6s	-10.10	2.28			
	6p	-6.86	2.241			
	5d	-12.10	4.762	1.938	0.6815	0.5774

[a] Contraction coefficients used in the double-ζ expansion.

pounds are so far unknown (see Table I), although attempts to obtain them were not abandoned until recently.[1-3,6,10] The same situation exists for the borides MB_2 with the AlB_2 crystal structure for d^5-d^{10} metals.[14]

Our calculations of the net charge in the hypothetical symmetrized Ta_3B_4 structure indicate that the largest negative net charge (-1.21) is located on the lateral Ta_2 atoms (see **15**), the Ta_1 atoms bearing smaller negative charge (-0.765). Thus the lateral site should be preferred for a more electronegative substituent than Ta, from the point of view of the topological charge stabilization rule.[48,50] In the case of ternary borides $MoCo_2B_4$,[62] $MoRu_2B_4$,[51] $MoMn_2B_4$,[63] $MoFe_2B_4$,[64] WMn_2B_4,[65] and other TMB with the Ta_3B_4 structure, these should be more stable with the more electronegative metal atom occupying the 4(g) site, in comparison with compound W_2FB_2,[65] Mo_2FeB_4,[10] and W_2MnB_4,[10] in which the stoichiometry does not permit the more electronegative atom to occupy the 4(g) site. These considerations do not take into account a variation in the valence electron count.

Acknowledgment. This research was supported by the National Science Foundation via Grant CHE-8912070. We thank Jane Jorgensen and Elisabeth Fields for their expert drawings.

Appendix

All the calculations are of the extended Hückel type, with a tight-binding approach.[26] The atomic parameters for H, B, and Ta atoms are listed in Table VI. The k point set used for the calculation of average properties consists of 18k points and was chosen according to the method of Ramirez and Böhm.[66]

Registry No. Ta_3B_4, 12045-92-0.

(63) Ishi, T.; Shimado, M.; Koizumi, M. *Inorg. Chem.* **1982**, *21*, 1670.
(64) Kuz'ma, Yu. B.; Nuch, O. V.; Skolodra, R. V. *Izv. AN* USSR, *Inorg. Mater.* **1966**, *2*, 1975.
(65) (a) Haschke, H.; Nowotny, H.; Benesovsky, F. *Monatsh. Chem.* **1966**, *B97*, 1459. (b) Kuz'ma, Yu. B.; Chepiga, M. V. *Izv.* AN USSR, *Inorg. Mater.* **1969**, *5*, 49.
(66) Ramirez, R.; Böhm, M. C. *Int. J. Quant. Chem.* **1986**, *30*, 391.

Temperature Behavior of an ESR Copper(II) Ion Pairs Spectrum Formed by Two Nonequivalent Cu^{2+} Ions

Antoine Abou Kais,* Rafeh Bechara, Cossi Faustin Aissi, and Michel Guelton

Université des Sciences et Techniques de Lille Flandres-Artois, Laboratoire de Catalyse Hétérogène et Homogène, URA CNRS No. 402, Bâtiment C3, 59655 Villeneuve d'Ascq Cédex, France

Received December 17, 1990. Revised Manuscript Received March 4, 1991

Copper-thorium oxides (Cu/Th > 0.25) prepared by coprecipitation of hydroxides and calcination at 1073 K contain Cu^{2+} ion pairs. Since the two ions are nonequivalent, the ESR parameters of the dimer spectrum change with the recording temperature. No correlation exists between the ESR spectra of the dimer and the single ion as its precursor.

Introduction

In previous work[1-4] it has been shown that the Cu^{2+} ions, occupying different sites in the CuThO catalysts, exhibit different behaviors and reactivities toward hydrogen and/or oxygen treatment.

For a low copper content (Cu/Th < 0.01), the Cu^{2+} ions, occupying substitutional (S) sites both on the surface (S_s or A_1 signal) and in the bulk (S_b or A_2 signal) of the CuThO solids were not susceptible to hydrogen reduction even at high temperature (873 K). On the other hand, for atomic ratios Cu/Th > 0.25, the Cu^{2+} ions, occupying sites on the catalysts surface (M_1, M_2, and D signals), were easily reduced by hydrogen. In the case of the copper(II) ion pairs (D signal) only one of the Cu^{2+} ions was susceptible to the redox treatment, whereas the other one, corresponding to the Cu^{2+} ion in the substitutional surface (S_s) site, remained stable toward the reagents.

The results mentioned above have been obtained from the ESR spectra recorded only at room temperature (293 K). Therefore, it is interesting to study the behavior of Cu^{2+} ions in the CuTh oxides at low temperature (77 K) and, in particular, the copper(II) ion pairs.

Experimental Part

The different solids were prepared at room temperature by coprecipitation of hydroxides by ammonium hydroxide from copper and thorium nitrates up to pH = 6.0. The CuTh oxides were obtained by calcination of the coprecipitated hydroxides at 1073 K for 5 h in a flow of dried air. Samples with different Cu/Th atomic ratios were prepared.

ESR spectra were obtained with a Bruker ER 200D spectrometer operating at X band (9.3 GHz) and using 100-kHz modulation. The spectra were recorded at 77 and 293 K. The g values were measured relative to "strong pitch": $g = 2.0028$.

Results and Discussions

Figure 1 shows the ESR spectra recorded at 77 K for CuTh oxides in the oxidized state with different atomic

* To whom correspondence should be addressed.

(1) Bechara, R.; Wrobel, G.; Aissi, C. F.; Guelton, M.; Bonnelle, J. P.; Abou Kais, A. *Chem. Mater.* **1990**, *2*, 518.
(2) Bechara, R.; D'Huysser, A.; Aissi, C. F.; Guelton, M.; Bonnelle, J. P.; Abou Kais, A. *Chem. Mater.* **1990**, *2*, 522.
(3) Bechara, R.; Abou Kais, A.; Guelton, M.; D'Huysser, A.; Grimblot, J.; Bonnelle, J. P. *Spectrosc. Lett.* **1990**, *23*(10), 1237.
(4) Abou Kais, A.; Bechara, R.; Ghoussoub, D.; Aissi, C. F.; Guelton, M.; Bonnelle, J. P. *J. Chem. Soc., Faraday Trans.* **1991**, *87*(4), 631.

0897-4756/91/2803-0557$02.50/0